Journal of Science and Technology in Civil Engineering, HUCE, 2023, 17 (2): 193–202

STUDY OF DYNAMIC RESPONSE OF CRANE SYSTEM VIA SURROGATES BASED ON KARHUNEN–LOÈVE EXPANSION AND NEURAL NETWORKS

Van-Hai Trinh[a,*]

[a]*Institute of Vehicle and Energy Engineering (IVEE), Le Quy Don Technical University, 236 Hoang Quoc Viet Street, Bac Tu Liem, Hanoi, Vietnam*

Article history:
Received 15/5/2023, Revised 25/6/2023, Accepted 25/6/2023

Abstract

Overhead cranes are widely used in construction sites and manufacturing/assembly lines for various tasks (loading, unloading, lifting, transporting,...). This paper investigates the dynamic response of the main beam (i.e., girder) of an overhead crane by a surrogate technique based on truncated Karhunen–Loève (KL) expansion and neural networks. First, the physical modeling and the motion equations of the crane system are derived using the Lagrange equation. Then, the dynamic responses of the overhead crane system with a number of the input parameters (i.e., configurations) are estimated by the numerical Newmark-beta integral method. Finally, the surrogates based on the truncated KL expansion and neural networks are constructed for studying the dynamic responses of the girder within a limited reference dataset. It can be stated that with a convergence property, the reconstructed surrogate performs good predictability for characterizing the dynamic responses of the structure. The presented method allows us to study the dynamic analysis and optimization of the crane according to the design conditions in the actual applications.

Keywords: overhead crane; dynamic response; surrogate model; Karhunen–Loève expansion; neural networks.

https://doi.org/10.31814/stce.huce2023-17(2)-17

1. Introduction

Overhead cranes (also known as bridge cranes) are essential in manufacturing lines because of their potential functions such as loading, unloading, lifting, moving,... The crane system is equipped with three independently guided working mechanisms including a bridge transfer mechanism, a winch transfer mechanism and an upgrade mechanism that allows the shaft to work efficiently within the working range of the crane hook [1–3]. With the advantages of their function and structure, factory cranes in particular and bridge cranes in general (including gantry cranes) have been interested in research to develop and perfect according to the requirements set out in practice. In which, the research focuses on solving two main groups of problems including: (i) dynamics and control [1, 4–7]; (ii) durability and structure [8–10]. The research methods used can be analytical method [5, 6, 10], numerical method (i.e., finite element method, FEM) [8, 9], and experimental method [7, 11].

In Ref. [12], Zrnić et al. has summarized some vibration models of cranes. A typical model for studying crane vibration has been built in the literature [5, 6]. In this model, assumptions such as the vehicle moving at a constant speed, the swing angle of the lift being small enough, and infinitely small quantities of the higher order are ignored. In the study [8], the authors have shown the influence of the trolley travel speed and the spring stiffness on beam deflection and a comparison between static and dynamic deflection was given for different trolley speeds. To study the oscillations of cranes with suspended control cabins taking into account these factors at the same time, the work [13] has

*Corresponding author. *E-mail address:* hai.tv@lqdtu.edu.vn (Trinh, V.-H.)

proposed a general vibration model of the crane in three-dimensional space, the links are connected by spring and damping element. The problem of completing and optimizing the steel structure of the crane and especially the main girder is mentioned in several published works [14, 15].

It can be stated that, for the more complex systems, we need to characterize or solve the design and optimization problems with a higher number of configurations in high-dimensional designing space. Typically, these tasks require reconstructing a meta-model (also known as surrogate model) [16–18] using polynomial approximations or machine learning techniques to enrich the data regarding the output responses of the system (i.e., input/output maps).

In this paper, the overhead crane's dynamic behavior is characterized in which the model parameters vary within a specific range. Regarding this, the fully referenced data is first estimated by the numerical Newmark-beta method. Then, the surrogate model based on neural networks is reconstructed using the truncated KL representation (i.e., the computational reduced coordinates) with a reasonable convergence property.

2. Dynamic model of overhead crane system

Fig. 1 depicts the two-dimensional dynamic model of a typical industrial overhead crane. This crane model consists of three main parts (bridge girder, trolley and payload) described as follows:

The crane girder is described by the elastic girder and only vertical vibrations are considered. The main girder has four descriptive parameters including: the distributed mass m_b, the overall length L, the elastic modulus E and the bending moment of inertia of the cross section I.

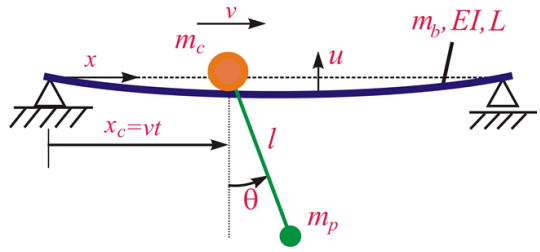

Figure 1. Dynamic model of an overhead crane system within a simply supported beam subject to a moving mass and a swing payload

The trolley of the crane is considered as a point mass with two described factors: the mass m_c and the moving speed v.

It is assumed that the payload (having a mass of m_p) swings with an angle θ and the rope length of l. Herein, the payload cable is considered to be a fixed-length element without mass during the transportation process.

Vibrations of the crane girder in the vertical plane passing through the beam axis can be approximated as follows [19]:

$$u(x,t) = \sum_{i=1}^{N} \phi_i(x) q_i(t), \quad \text{with } \phi_i(x) = \sin\left(\frac{i\pi x}{L}\right) \tag{1}$$

where ϕ_i is the i^{th} modal shape of the crane beam, $q_i(t)$ are the generalized coordinates of the beam displacement, and N is the total number of modes under consideration.

To establish the differential equation describing the system motion, we first find the total kinetic energy T and the total potential energy V of the crane system [2].

The total kinetic energy is estimated as:

$$\begin{aligned} T = {} & \frac{1}{4} m_b L \sum_{i=1}^{N} \dot{q}_i^2 + \frac{1}{2} m_c \left\{ \dot{x}_c^2 + \left[\dot{x}_c \sum_{i=1}^{N} \phi_i'(x_c) q_i(t) + \sum_{i=1}^{N} \phi_i(x_c) \dot{q}_i(t) \right]^2 \right\} \\ & + \frac{1}{2} m_p \left\{ \left(\dot{x}_c + \dot{\theta} l \cos\theta \right)^2 + \left[\dot{x}_c \sum_{i=1}^{N} \phi_i'(x_c) q_i(t) + \sum_{i=1}^{N} \phi_i(x_c) \dot{q}_i(t) - \dot{\theta} l sin\theta \right]^2 \right\} \end{aligned} \tag{2}$$

The total potential energy is calculated by:

$$V = \frac{EI\pi^4}{4L^3}\sum_{i=1}^{N} i^4 q_i^2(t) - m_c g u(x_c,t) - m_p g\left[u(x_c,t) + l(\cos\theta - 1)\right] \tag{3}$$

Using the Lagranges equation for the non conservative systems, the differential equation of the system motion is formulated in the following equation:

$$\boldsymbol{M}\ddot{\boldsymbol{u}} + \boldsymbol{K}\dot{\boldsymbol{u}} + \boldsymbol{C}\boldsymbol{u} = \boldsymbol{P} \tag{4}$$

where $\boldsymbol{M}$, $\boldsymbol{C}$, and $\boldsymbol{K}$ are the system mass, damping, and stiffness matrices of size $(N{+}1)\times(N{+}1)$; $\boldsymbol{P}$ is the time-dependent loading vector having a size of $N{+}1$; $\boldsymbol{u} = [u_i]_{(N+1)\times 1} = [\theta, q_1, q_2, \ldots, q_N]^T$ is the displacement vector, whereas $\ddot{\boldsymbol{u}}$ and $\dot{\boldsymbol{u}}$ are the acceleration and velocity vectors.

The above matrices and vectors are detailed in Eq. (5), see Appendix A in Ref. [2] for their expansion formulas:

$$\begin{aligned}
\boldsymbol{M} &= \begin{bmatrix} m_p l^2 & -2m_p l\sin\theta[\phi_i(x_c)] \\ -2m_p l\sin\theta[\phi_i(x_c)]^T & \dfrac{m_b L}{2}[\mathbf{I}]_{N\times N} + 2\left(m_p + m_c\right)\mathrm{diag}[\phi_i(x_c)][\phi_i(x_c)] \end{bmatrix} \\
\boldsymbol{K} &= \begin{bmatrix} \dfrac{m_p g l\sin\theta}{\theta} & -2m_p l\sin\theta\left\{\ddot{x}_c[\phi_i'(x_c)] + \dot{x}_c^2[\phi_i''(x_c)]\right\} \\ [\mathbf{0}]_{N\times 1} & \mathrm{diag}[\dfrac{EI\pi^4 i^3}{2L^3}] + 2\left(m_p + m_c\right)\left\{\begin{array}{l} \ddot{x}_c\mathrm{diag}[\phi_i(x_c)][\phi_i'(x_c)] \\ +\dot{x}_c^2\mathrm{diag}[\phi_i(x_c)][\phi_i''(x_c)] \end{array}\right\} \end{bmatrix} \\
\boldsymbol{C} &= \begin{bmatrix} 0 & -2m_p l x_c\cos\theta[\phi_i'(x_c)] \\ -2m_p l x_c\sin\theta[\phi_i'(x_c)]^T & 2\left(m_p + m_c\right)\dot{x}_c\mathrm{diag}[\phi_i(x_c)][\phi_i'(x_c)] \end{bmatrix} \\
\boldsymbol{P} &= \begin{bmatrix} -m_p\ddot{x}_c l\cos\theta & (m_p + m_c)[\phi_i(x_c)]^T \end{bmatrix}
\end{aligned} \tag{5}$$

where $[\phi_i]$ is a $N{\times}N$ matrix consisting of N identical row of $[\phi_i]_{1\times N} = \begin{bmatrix} \phi_1 & \phi_2 & \ldots & \phi_N \end{bmatrix}$, matrices $[\phi_i']$ and $[\phi_i'']$ are the first and second partial derivatives of the matrix with respect to the variable x_c, respectively. The notation $\mathrm{diag}(\phi_i)$ is a diagonal matrix with the elements on the diagonal being the elements of the vector $[\phi_i]$, $[\mathbf{I}]_{N\times N}$ is the unit matrix.

The numerical Newmark-beta method is employed to solve Eq. (4). Regarding this, the acceleration and velocity vectors ($\ddot{\boldsymbol{u}}$ and $\dot{\boldsymbol{u}}$) of the crane girder at the time $(t + \Delta t)$ can be calculated according to the corresponding known values at the time t by the following equations [20]:

$$\begin{aligned}
\ddot{\boldsymbol{u}}(t+\Delta t) &= a_0\left[\boldsymbol{u}(t+\Delta t) - \boldsymbol{u}(t)\right] - a_2\dot{\boldsymbol{u}}(t) - a_3\ddot{\boldsymbol{u}}(t) \\
\dot{\boldsymbol{u}}(t+\Delta t) &= \dot{\boldsymbol{u}}(t) + a_6\ddot{\boldsymbol{u}}(t) + a_7\ddot{\boldsymbol{u}}(t+\Delta t)
\end{aligned} \tag{6}$$

in Eq. (6), the displacement vector $\boldsymbol{u}(t + \Delta t)$ is defined by:

$$\begin{aligned}
\boldsymbol{u}(t+\Delta t) &= \tilde{\boldsymbol{K}}(t+\Delta t)\backslash\tilde{\boldsymbol{P}}(t+\Delta t) \\
\tilde{\boldsymbol{K}}(t+\Delta t) &= \boldsymbol{K}(t) + a_0\boldsymbol{M}(t) + a_1\boldsymbol{C}(t) \\
\tilde{\boldsymbol{P}}(t+\Delta t) &= \boldsymbol{P}(t+\Delta t) + \boldsymbol{M}(t)\left[a_0\boldsymbol{u}(t) + a_2\dot{\boldsymbol{u}}(t) + a_3\ddot{\boldsymbol{u}}(t)\right] \\
&\quad + \boldsymbol{C}(t)\left[a_1\boldsymbol{u}(t) + a_4\dot{\boldsymbol{u}}(t) + a_5\ddot{\boldsymbol{u}}(t)\right]
\end{aligned} \tag{7}$$

and some coefficients introduced in the above equations are selected as:

$$a_0 = \frac{1}{\beta\Delta t^2};\ a_1 = \frac{\gamma}{\beta\Delta t^2};\ a_2 = \frac{1}{\beta\Delta t};\ a_3 = \frac{1}{2\beta} - 1;\ a_4 = \frac{\gamma}{\beta} - 1$$
$$a_5 = \frac{\Delta t}{2}\left(\frac{\gamma}{\beta} - 1\right);\ a_6 = \Delta t(1-\gamma);\ a_7 = \gamma\Delta t \tag{8}$$
$$\beta = \frac{1}{4};\ \gamma = \frac{1}{2}$$

3. Construction of surrogates model

3.1. Karhunen–Loève expansion

In this section, we seek a surrogate model that maps some system parameters (i.e., material or structural factors) to the dynamic response over the investigation time denoted by $t \in T$. Let $\tau = \tau(t, \boldsymbol{\mu})$ represent the forward map of interest and $\boldsymbol{\mu}$ be the input parameters vector. Below this response is written simply by $\tau = \tau(t)$. The response $\tau(t)$ can be represented through the Karhunen-Loève expansion [21],

$$\tau(t) = \bar{\tau}(t) + \sum_{i=1}^{+\infty} \sqrt{\lambda_i}\eta_i\varphi_i(t) \tag{9}$$

where $\bar{\tau}(t)$ is the mean function of the dynamics response and the pairs $\{(\lambda_i, \varphi_i)\}_{i\geq 1}$ are the covariance operator's eigenvalues and eigenfunctions that satisfy the following integral equation:

$$\int_T C(t,t')\phi_i(t')\,dt' = \lambda_i\varphi_i(t) \tag{10}$$

where $C(t,t')$ is the covariance function, and the reduced variables are defined as:

$$\eta_i = \frac{1}{\sqrt{\lambda_i}}\langle \tau(t) - \bar{t}(t), \varphi_i(t)\rangle \tag{11}$$

Herein, it can be noted that the variables $\{\eta_i\}_{i\geq 1}$ are centered and pairwise uncorrelated and having unit variance. The operator $\langle f(t), g(t)\rangle$ is the inner product between functions:

$$\langle f(t), g(t)\rangle = \int_T f(t)\,g(t)\,dt \tag{12}$$

The truncated expansion can be written in the form:

$$\tau(t) = \bar{\tau}(t) + \sum_{i=1}^{p} \sqrt{\lambda_i}\eta_i\varphi_i(t) \tag{13}$$

herein, p is the truncated order defined through a convergence analysis $\left(\lim_{p\to+\infty} \tau_p = \tau\right)$.

Next, the convergence property of the truncated KL expansion is characterized via two error functions. First, we determine the number of realizations that are needed to reach the convergence by measuring the function $N_s \mapsto \mathrm{Cov}(N_s)$ as:

$$\mathrm{Cov}(N_s) = \left\|\left[\tilde{C}(N_s)\right]\right\| \tag{14}$$

in which, $\tilde{C}$ is the covariance matrix of the discretized process.

To identify the truncated order p in the statistical estimator, we then measure the convergence by the error map $p \mapsto \mathrm{Err}(p)$ as:

$$\mathrm{Err}(p) = 1 - \frac{\sum_{i=1}^{p}\lambda_i}{\mathrm{tr}\left(\left[\tilde{C}\right]\right)} \tag{15}$$

3.2. Neural network architecture

Fig. 2 shows the reconstructed neural network (NN) architecture that consists of n_L layers including an input layer, some hidden layers, and an output layer. The number of neurons in the l^{th} layer is denoted by $n^{(l)}$. Here, $n^{(1)} = 5$ and $n^{(nL)} = p$, while these numbers of the hidden layers (i.e., $n^{(2)}$and $n^{(3)}$) are chosen to ensure a good generalization. Noted that these counts of neurons exclude the biases or the last neuron denoted by (+1). Let $\boldsymbol{\mu}^{(i)} = (EI^{(i)}, m_b{}^{(i)}, m_c{}^{(i)}, m_p{}^{i)}, l_p{}^{(i)})^T$ be the input vector for a data point i, and $\boldsymbol{\eta}^{(i)}$ be the reduced variables in KL expansion used for representing the output response $\boldsymbol{\tau}$. The main aim is to find a network structure, in which the input/output relationship is better formulated based on the dataset, $\boldsymbol{S} = [(\boldsymbol{\mu}^{(i)}, \boldsymbol{\eta}^{i)})| \, i \in [1, \ldots, N_s]]$, with N_s is the sampling size.

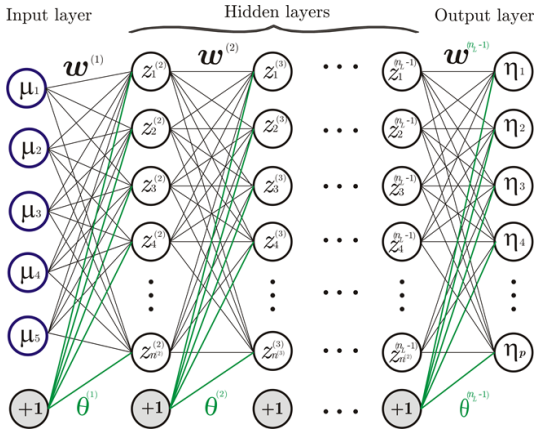

Figure 2. Reconstructed neural network architecture for the dynamic system. The number of neurons in the input layer and output layers are five crane input parameters and the order of the truncated KL expansion, respectively

To begin with, in a given layer, the output of the j^{th} neuron is produced by:

$$z_j^{(l+1)} = f\left(\sum_{i=1}^{n^{(l)}} w_{ij}^{(l)} z_j^{(l)} + \theta_j^{(l)}\right), \text{ with } l = 1, \ldots, n_L - 1 \text{ and } z_i^{(l)} = \mu_i \tag{16}$$

herein, $f(\cdot)$ is the activation or transfer function (in this work, the used sigmoid function given as $f(v) = 1/[1 + \exp(-v)]$. Alternatively, there are other functions commonly used, e.g., the hyperbolic tangent). $w_{ij}^{(l)} z_j^{(l)}$ is the weighted sum of input signals and $\theta_j^{(l)}$ is the bias. Thus, the connectivity between two layers can be represented by a weight matrix $\boldsymbol{w}^{(l)} = [w_{lk}^{(l)}]_{n^{(l)} \times n^{(l+1)}}$ and a bias vector $\boldsymbol{\theta}(l) = [\theta_k^{(l)}]_{1 \times n}{}^{(l+1)}$.

Consequently, with a given input data and a set of weights $\boldsymbol{w} = (\boldsymbol{w}^{(1)}, \ldots, \boldsymbol{w}^{(nL-1)})$ and biases $\boldsymbol{\theta} = (\boldsymbol{\theta}^{(1)}, \ldots, \boldsymbol{\theta}^{(nL-1)})$, the predictions of the NN model, denoted by $\hat{\boldsymbol{\eta}}_{w,\theta}\left(\boldsymbol{\mu}^{(i)}\right)$, are produced. Obviously, the objective is to find the best weights $\boldsymbol{w}$ and the biases $\boldsymbol{\theta}$ that minimize the loss or error function between the predicted and reference values. The L_k-norm loss function can be estimated as:

$$L(\boldsymbol{w}, \boldsymbol{\theta}) = \frac{1}{N_s} \sum_{i=1}^{N_s} \left\| \hat{\boldsymbol{\eta}}_{w,\boldsymbol{\theta}}\left(\boldsymbol{\mu}^{(i)}\right) - \boldsymbol{\eta}^{(i)}) \right\|^k, \; k = 1, 2 \tag{17}$$

A new iteration of the learning process proceeds to minimize $L(\boldsymbol{w},\theta)$ that compares the predicted outputs with the target or the reference values. Using the Levenberg–Marquardt optimization method for training, in a general form, the weights and bias are updated as [22, 23],

$$\boldsymbol{w}^{(k+1)} = \boldsymbol{w}^{(k)} - \left[\boldsymbol{J}^T \boldsymbol{J} + \mu \boldsymbol{I}\right]^{-1} \boldsymbol{J}^T \boldsymbol{e} \tag{18}$$

where the collection $\boldsymbol{w}$ contains all of the weights and biases mentioned earlier, μ denotes the learning rate, and $\boldsymbol{I}$ is the identity matrix. $\boldsymbol{J}$ is the Jacobian matrix that collects all first derivatives of the error patterns with respect to the weights and bias. The error vector, denoted by $\boldsymbol{e}$, is computed for each learning iteration, k.

In this work, the design and training of the NN model are performed with the Neural Network MATLAB toolbox [24]. The dataset of the NN model typically consists of a collection of raw data, thus a normalization step is necessary to make sure that the data is in the same range of the transfer function. For the case of the standard sigmoid (i.e., data in the range of [0, 1]), the minimum and maximum values of the raw data are used to normalize them as [25].

$$x_i = \frac{x_i - x_{\min,i}}{x_{\max,i} - x_{\min,i}} \tag{19}$$

4. Results and discussion

4.1. Fully reference data and reduced coordinates

To generate the reference data of the dynamic behaviour of the crane system, we consider $\boldsymbol{\mu} = [\mu_i]_{1\times 5} = \left[\begin{array}{ccccc} EI & m_b & m_c & m_p & l \end{array}\right]$ as the vector of the random input parameters. In this work, random variables μ_i are independent and following the standard normal distribution with the mean value $\bar{\mu}_i$ and random factors γ_i as $\mu_i = \bar{\mu}_i(1 + \gamma_i)$ in which γ_i is formulated by $\bar{\gamma}$ and the deviation $\sigma_\gamma = 0.1$. This paper uses the crane configuration of the follow parameters [3, 5]: $\overline{EI} = 4.50\times10^4$ Nm^2, $\bar{m}_b$ = 163.2 kg/m, $\bar{m}_c = \bar{m}_p = 97.9$ kg/m, $\bar{l} = 2$ m, and $L = 6$ m. Herein, at the initial time $t = 0$: $\theta(0)$ = - 0.01 rad, $\dot{\theta}(0) = 0$; and $q_i(0) = 0$, $\dot{q}_i(0) = 0$ with $i = 1, \ldots, N$. The trolley speed is $v = 0.4$ m/s during the crane working process.

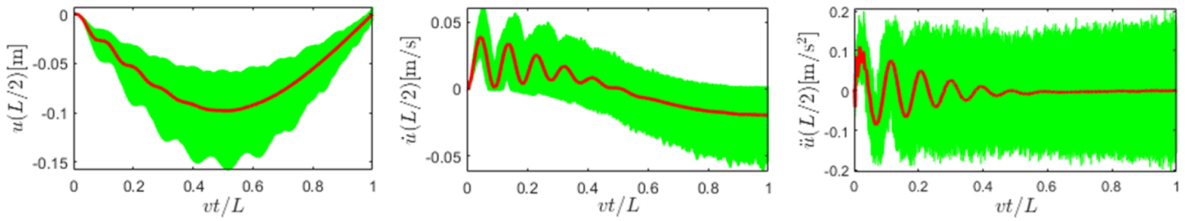

(a) Displacement (b) Velocity (c) Acceleration

Figure 3. The results of crane dynamic response of the girder beam midpoint ($x_c = L/2$)

Fig. 3 shows the obtained dynamic response of the overhead crane through the displacement (a), the velocity (b), and the acceleration (c) of the girder beam midpoint ($x = L/2$). On these subfigures, the central bold line is the mean value, and the shaded area is formed from the maximum and minimum value boundaries at each calculation time. Note that the total number of the crane configurations is $N_s = 10^3$, and the value of time step in the Newmark-beta procedure is selected Δt = 0.01 (i.e., $N = 1500$). In the following parts, we will use the displacement response as the reference data for the truncated KL expansion in what follows.

Fig. 4(a) and Fig. 4(b) show the graphs of the function $N_s \mapsto \mathrm{Cov}\,(N_s)$ and the error function $p \mapsto \mathrm{Err}(p)$, respectively. It is found that for the number of realizations, $N_s = 1000$ we can achieve a reasonable convergence. For the convergence with the truncated order, the error is less than 1e-3 (respectively 1e-4 and 1e-5) for $p = 10$ (respectively $p = 12$ and $p = 15$). Thus, in what follows, we consider a truncation at order $p = 10$ and a realization number of $N_s = 1000$.

The graphs of the first five eigenfunctions $\{\phi_i(t)\}_{i=1}^5$ are plotted in Fig. 5. Using these five eigenfunctions, for a specific crane configuration, a quantitative comparison between the reference displacement response and the truncated KL expansion is provided in Fig. 6. From the obtained tracking between the reference curve and the KL curve, it can be stated that the truncated KL expansion presents well the generated reference data.

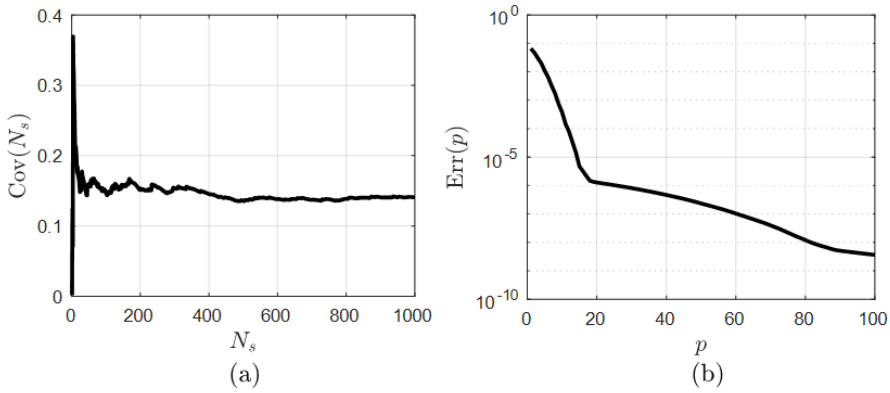

Figure 4. Convergence properties of the truncated KL representation

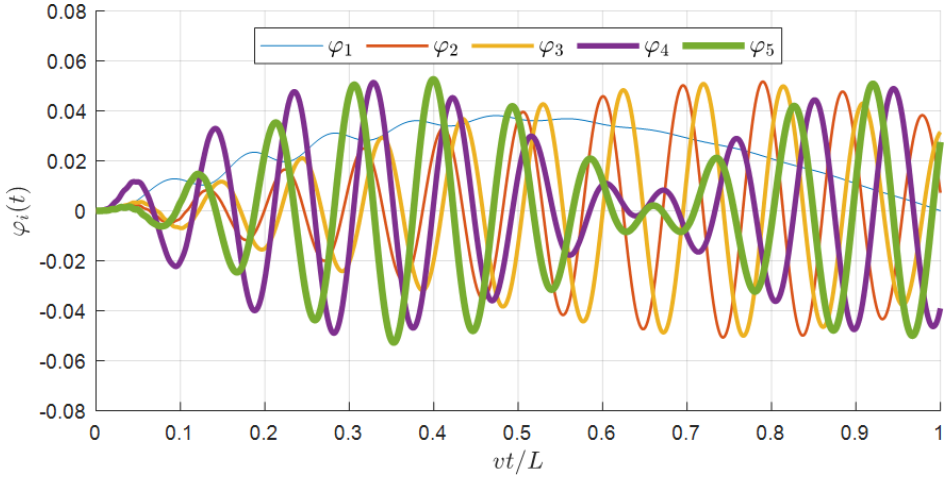

Figure 5. The five first eigenfunctions are used for representation of the displacement response of the crane girder

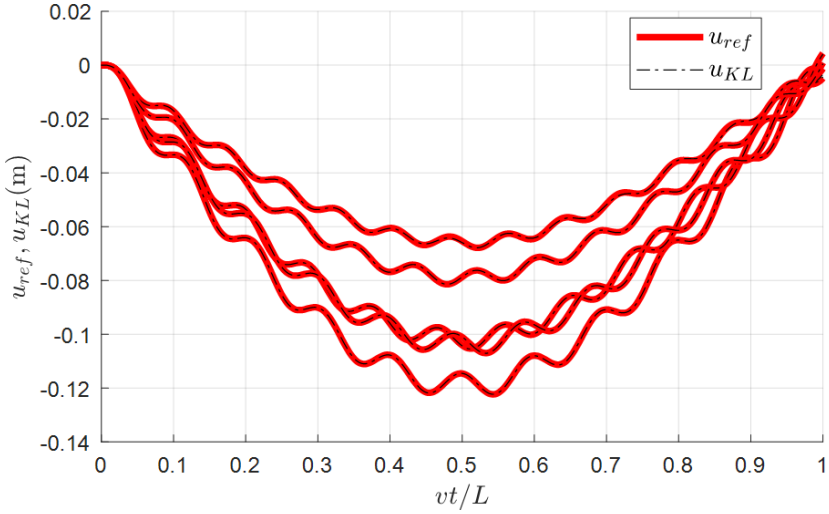

Figure 6. Graphs of the reference function (thick line) and KL approximation (dot-dash thin line) for five configurations of the crane girder

4.2. Assessments of surrogate performance

In this section, the computational reduced coordinates ($\boldsymbol{\eta}$) is approximated by the reconstructed neural network with $n^{(1)} = 5$ neurons for input layer and $n^{(nL)} = 10$ neurons for output layer. While no attempt was made to fully optimize the reconstructed architecture, a four-hidden-layers network (within p neurons per layer) was provided to obtain reasonably accurate results. In order to generate the data for the training and examining process of the NN model, we calculate a number of 1000 random cases (corresponding to $N_s = 1000$ sets of the input parameters of the crane girder).

In the training process, the convergence of the mean squared error for the training, validation, and testing dataset is shown in Fig. 7(a), and their neural network regression results are plotted in Fig. 7(b) to Fig. 7(d), respectively. Herein, a total of 950 configurations is considered (training dataset: 760 configurations, validation dataset: 95 configurations, and testing dataset: 95 configurations). It can be noted that the best validation performance occurs at iteration 130, and the achieved mean squared error on three datasets is less than 10^{-4} (see Fig. 7(a)). This low value can ensure that the prediction of the surrogates is highly accurate.

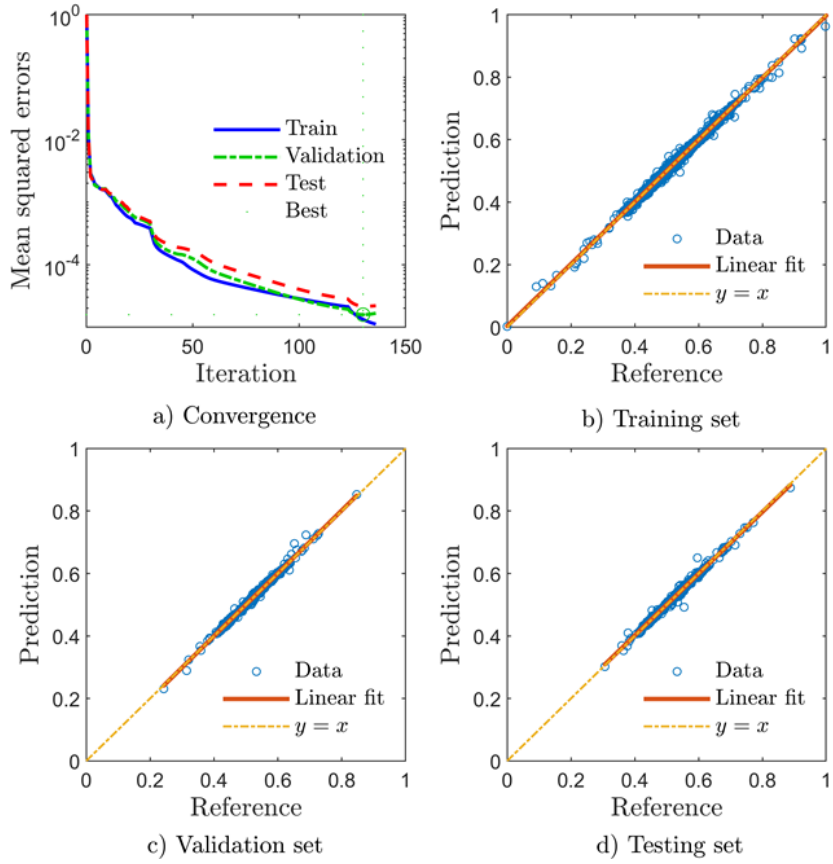

Figure 7. Performance of the reconstructed neural network architecture: convergence of the mean squared errors (a), and neural network regression results (b-d) for three dataset (i.e., training, validation, and testing, respectively)

When the dataset is being examined, it is not taken into account during the training process. The prediction performance of the generated NN surrogate with a number of given configurations (i.e., 50 configurations) is provided in Figs. 8–9. For some illustrated configurations under consideration, it is found that the surrogate model predicts dynamic behavior highly accurately over the whole time

domain (Fig. 8). Additionally, the achieved performance of the surrogate model is also confirmed by the comparison between the reference and the NN prediction value of 75050 points of dynamic response with a high R-square value of 0.9997 (see Fig. 9).

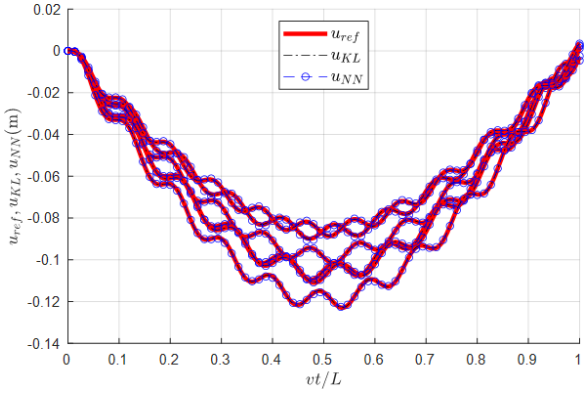

Figure 8. Predictability of the NN network for new dataset of dynamic response for 5 configurations of the random input parameters: reference function (thick line) and KL approximation (dot-dash thin line), and NN prediction (circle markers)

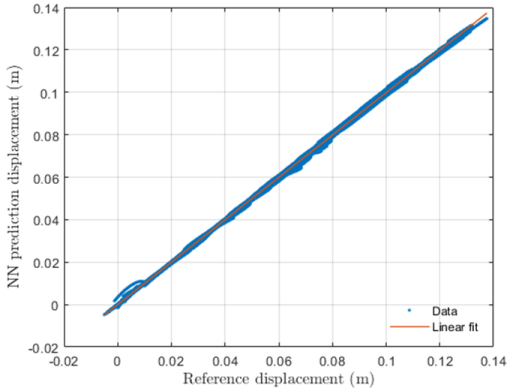

Figure 9. Predictability of the NN network for a dataset of 50 girder configurations

In term of computation cost, for a case of 1000 computation configurations ensuring a convergence feature, the total computation time for the numerical simulations is about 800 seconds, whereas the constructed NN model (within the training time around 160 seconds) is able to complete the task within the same number of configurations in less than 0.3 seconds which low consumption can be beneficial for either increasing the computation grid points or the integrating the dynamic problem as a call function in a complex computing scheme (e.g., optimization).

5. Conclusions

The present paper reconstructed the surrogate model based on KL expansion and neural networks to describe the dynamic responses of the overhead crane system. The NN architecture is trained with data consisting of the computational reduced coordinates (i.e., the truncated KL expansion) which are computed from the reference dynamic response (focusing on the displacement response). Utilizing the proposed method enables to significantly reduce the computational cost. In terms of predictability, the NN model shows a good performance for the new data with an R-square value of nearly one. Thus, the surrogate model allows the cost function to be evaluated at a negligible computational expense, which opens up many possibilities to design and optimize the cane system under constraints related to different dynamic parameters.

Acknowledgements

The authors are enormously grateful to Johann Guilleminot (Duke University, Durham, USA) for discussions regarding the KL expansion.

References

[1] Hong, K.-S., Shah, U. H. (2019). *Dynamics and Control of Industrial Cranes*. Springer Singapore.

[2] Liu, H., Cheng, W., Li, Y. (2019). Dynamic Responses of an Overhead Crane's Beam Subjected to a Moving Trolley with a Pendulum Payload. *Shock and Vibration*, 2019:1–14.

[3] Xin, Y., Xu, G., Su, N., Dong, Q. (2018). Nonlinear Vibration of Ladle Crane due to a Moving Trolley. *Mathematical Problems in Engineering*, 2018:1–14.

[4] Chen, Q., Cheng, W., Gao, L., Du, R. (2020). Dynamic Response of a Gantry Crane's Beam Subjected to a Two-Axle Moving Trolley. *Mathematical Problems in Engineering*, 2020:1–10.
[5] Oguamanam, D. C. D., Hansen, J. S., Heppler, G. R. (2001). Dynamics of a three-dimensional overhead crane system. *Journal of Sound and Vibration*, 242(3):411–426.
[6] Oguamanam, D. C. D., Hansen, J. S., Heppler, G. R. (1998). Dynamic response of an overhead crane system. *Journal of Sound and Vibration*, 213(5):889–906.
[7] Toxqui, R., Yu, W., Li, X. (2006). Anti-swing control for overhead crane with neural compensation. In *The 2006 IEEE International Joint Conference on Neural Network Proceedings*, IEEE, 4697–4703.
[8] Gašić, V., Zrnić, N., Obradović, A., Bošnjak, S. (2011). Consideration of moving oscillator problem in dynamic responses of bridge cranes. *FME Transactions*, 39(1):17–24.
[9] Patel, P. R., Patel, V. K. (2013). A review on structural analysis of overhead crane girder using FEA technique. *International Journal of Engineering, Science and Innovative Technology*, 2(4):41–44.
[10] Hai, T. V., Thu, N. H., Tuan, H. D., Hiu, P. V. (2020). Failure probability analysis of overhead crane bridge girders within uncertain design parameters. *Journal of Science and Technology in Civil Engineering (STCE) - HUCE*, 14(3):125–135.
[11] Arena, A., Casalotti, A., Lacarbonara, W., Cartmell, M. P. (2015). Dynamics of container cranes: three-dimensional modeling, full-scale experiments, and identification. *International Journal of Mechanical Sciences*, 93:8–21.
[12] Zrnić, N., Gašić, V., Bošnjak, S., Đorđević, M. (2013). Moving loads in structural dynamics of cranes: bridging the gap between theoretical and practical researches. *FME Transactions*, 41(4):291–297.
[13] Xin, Y., Xu, G., Su, N. (2017). Dynamic Optimization Design of Cranes Based on Human–Crane–Rail System Dynamics and Annoyance Rate. *Shock and Vibration*, 2017:1–19.
[14] Patel, H., Upadhyay, D., Patel, D. (2020). Design optimization of box girder in gantry crane using finite element analysis software. *International Research Journal of Engineering and Technology*, 7(08):1906–1917.
[15] Fan, X., Wang, P., Hao, F. (2019). Reliability-based design optimization of crane bridges using Kriging-based surrogate models. *Structural and Multidisciplinary Optimization*, 59(3):993–1005.
[16] Trinh, V.-H., Nguyen, V.-T., Pham, K.-Q. (2021). Global Sensitivity Analysis for Bridge Crane System by Surrogate Modeling. In *Lecture Notes in Civil Engineering*, Springer Nature Singapore, 285–293.
[17] Fan, X., Wang, P., Hao, F. (2019). Reliability-based design optimization of crane bridges using Kriging-based surrogate models. *Structural and Multidisciplinary Optimization*, 59(3):993–1005.
[18] Hung, D. V., Thang, N. T. (2022). Predicting dynamic responses of frame structures subjected to stochastic wind loads using temporal surrogate model. *Journal of Science and Technology in Civil Engineering (STCE) - HUCE*, 16(2):106–116.
[19] Yang, Y. B., Lin, C. W. (2005). Vehicle–bridge interaction dynamics and potential applications. *Journal of Sound and Vibration*, 284(1-2):205–226.
[20] Newmark, N. M. (1959). A Method of Computation for Structural Dynamics. *Journal of the Engineering Mechanics Division*, 85(3):67–94.
[21] Lord, G. J., Powell, C. E., Shardlow, T. (2014). *An Introduction to Computational Stochastic PDEs*. Cambridge University Press.
[22] Marquardt, D. W. (1963). An Algorithm for Least-Squares Estimation of Nonlinear Parameters. *Journal of the Society for Industrial and Applied Mathematics*, 11(2):431–441.
[23] Hagan, M. T., Menhaj, M. B. (1994). Training feedforward networks with the Marquardt algorithm. *IEEE Transactions on Neural Networks*, 5(6):989–993.
[24] Demuth, H. B., Beale, M. H. (1992). *Neural network toolbox user's guide*. Mathworks, Incorporated.
[25] Kim, D. (1999). Normalization methods for input and output vectors in backpropagation neural networks. *International Journal of Computer Mathematics*, 71(2):161–171.